Research Article | Vol. 61, No. 28 / 1 October 2022 / Applied Optics 8493

applied optics

Constant amplitude modulation heterodyne interferometry

HESHAN LIU,[1] JUAN WANG,[1,2] RUIHONG GAO,[1,3] AND ZIREN LUO[1,*]

[1]National Microgravity Laboratory (NML), Institute of Mechanics, Chinese Academy of Sciences, Beijing 100190, China
[2]School of Engineering Science, University of Chinese Academy of Sciences, Beijing 100049, China
[3]School of Fundamental Physics and Mathematical Sciences, Hangzhou Institute for Advanced Study, UCAS, Hangzhou 310024, China
*Corresponding author: luoziren@imech.ac.cn

Received 24 February 2022; revised 19 May 2022; accepted 31 July 2022; posted 12 September 2022; published 27 September 2022

Laser interferometer with picometer precision is a key technology in the space gravitational wave detection. Many interferometry strategies have been put forward for the multiple purposes in the past 10 yr. We propose a new interferometry method, called constant amplitude modulation (CAM) heterodyne interferometry. Differently, the CAM provides an optical pilot tone (OPT) for the noise correction theme. Compared with the analog pilot tone, the OPT can record and correct more noises, such as the analog to digital converter sampling jitter, the photodetector noise and the analog front-end noise. From the discussion, the modulated depth $\phi_{\text{modulate}} = 1.375$ rad and the power ratio of the beam split $n = 0.432$ are the best choice for the CAM-modulated parameter. Moreover, a simulated case has been implemented for the verification of the CAM strategy. Therefore, the CAM gives us another excellent choice in the optical design of the interferometer.

https://doi.org/10.1364/AO.456944

1. INTRODUCTION

Using the laser interferometry to measure the tiny displacement with picometer precision is a key technique in the space gravitational wave detection, such as the laser interferometer space antenna (LISA) [1] and the Taiji program [2]. Compared with the traditional heterodyne interferometry, several types of interferometry strategies [3,4], such as the digitally enhanced interferometry (DeI) [5–7], the deep phase modulation (DPM) [8] interferometry, and the deep frequency modulation (DFM) [9,10] interferometry have been proposed to measure multiple targets or simplify the complexity of the laser interferometer in the past 10 yr [11]. Through deeply modulating the phase of one interferometer arm, the beat note of the DPM can form multitones, which include the optical length information [8]. Similarly, the DFM deeply modulates the frequency of the laser to form the same multitones as the DPM [9]. Differently, multitones of the DFM only appear when the two arm lengths of the interferometer are unequal. The phase extraction method of the DPM and the DFM is more complicated [12] and totally different with the digital phase-locked loop (DPLL) [13,14] algorithm, which has been widely adopted in the space gravitational wave detection missions [15]. Based on the traditional interferometry, the DeI uses the electro-optic modulator to modulate the pseudorandom noise (PRN) code to the laser beam [6]. The PRN code gives the DeI ability to distinguish the motion of multitargets in the road of the beam transfer.

In this paper, we propose a new interferometry strategy, called the constant amplitude modulation (CAM) heterodyne interferometry. The CAM is an optimized choice of the deep amplitude modulation. Compared with typical heterodyne interferometry, the CAM deeply modulates the amplitude of one laser beam. Importantly, the CAM provides an optical signal, which is related to the modulated rf source and not to the optical path noise. That is to say, the CAM gives an optical pilot tone OPT for the theme of the noise correction, which is different with the rf analog pilot tone [13]. The OPT not only can calibrate the analog to digital converter (ADC) sampling jitter, but also can calibrate the noise of the photodetector and the analog front-end noise. Moreover, the phasemeter of the DPLL architecture also can be used in the CAM, which has been proven as the most suitable method for the space laser interferometer [15]. In the following, the theory of the CAM interferometry is first discussed. Then, the parameter of the CAM is discussed and given. Finally, a simulation case of the CAM is shown.

2. THEORY

For better explaining the CAM strategy, the typical optical layout is shown in Fig. 1. The amplitude modulation of a laser beam is always implemented by an electro-optic amplitude modulator (EOAM), which utilizes the character of the Mach–Zehnder interferometer. Changing the electric field on the phase modulating path of the EOAM will control the power of the exiting light. Therefore, the CAM is a more complex DPM

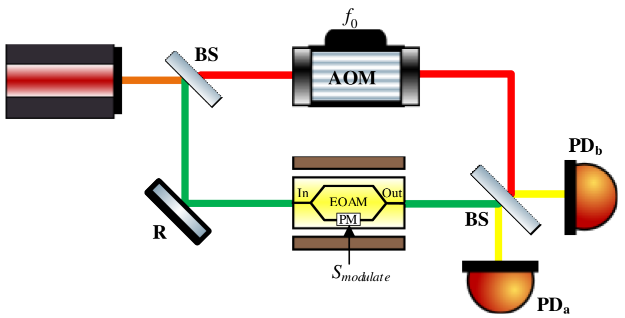

Fig. 1. Typical optical layout of the CAM interferometry. Beam splitter (BS), reflector (R), acoustic-optical modulator (AOM), photodetector (PD), and phase modulation (PM).

interferometer, which is the interference of three beams in the ending beat note.

In Fig. 1, one laser beam is first split into two by a BS. Then, one of the beams E_{Beam1} is frequency shifted with the value of f_0 by an AOM, and the other beam E_{Beam2} is amplitude modulated by an EOAM with the frequency f_{modulate}. The output beam modulated by the EOAM is the combination of two beams E_{EOAM1} and E_{EOAM2}. Lastly, three beams are interfered with each other. Assuming the value of the laser frequency is f, and three components of the interferometer could be described as

$$\begin{aligned} E_{\mathrm{Interference}} &= E_{\mathrm{Beam1}} + E_{\mathrm{EOAM1}} + E_{\mathrm{EOAM2}} \\ E_{\mathrm{Beam1}} &= A_{\mathrm{Beam1}} \cos\left(2\pi(f+f_0)t + \phi_{\mathrm{laserjitter}} + \phi_{\mathrm{path1}}\right) \\ E_{\mathrm{EOAM1}} &= A_{\mathrm{Beam2}} \Big/ \sqrt{2} \cos\left(2\pi f t + \phi_{\mathrm{laserjitter}} + \phi_{\mathrm{path2}}\right) \\ E_{\mathrm{EOAM2}} &= A_{\mathrm{Beam2}} \Big/ \sqrt{2} \cos\left(2\pi f t + \phi_{\mathrm{laserjitter}} \right. \\ &\qquad \left. + \phi_{\mathrm{path2}} + S_{\mathrm{modulate}}\right), \end{aligned} \tag{1}$$

where $E_{\mathrm{Interference}}$, E_{Beam1}, E_{Beam2}, E_{EOAM1}, E_{EOAM2} are the electric field of the related laser beam, respectively. A_{Beam1} and A_{Beam2} are the amplitude of the beam E_{Beam1} and E_{Beam2}. $\phi_{\mathrm{laserjitter}}$ is the frequency jitter of the laser beam. ϕ_{path1} and ϕ_{path2} represent the optical path noise of two arms of the interferometer in Fig. 1. $S_{\mathrm{modulate}} = \phi_{\mathrm{offset}} + \phi_{\mathrm{modulate}} \cos(2\pi f_{\mathrm{modulate}} t + \phi_{m0})$, where the ϕ_{offset}, ϕ_{modulate}, and ϕ_{m0} are the offset, amplitude, and initial phase of the phase modulation of the EOAM.

Therefore, the detected power by the PD of the interferometer can be written as

$$\begin{aligned} P_{\mathrm{out}} &\propto {E_{\mathrm{Interference}}}^2 \\ P_{\mathrm{out}} &= A^2_{\mathrm{Beam1}} \Big/ 2 + A^2_{\mathrm{Beam2}} \Big/ 2 \\ &\quad + A_{\mathrm{Beam1}} A_{\mathrm{Beam2}} \Big/ \sqrt{2} \cos\left(2\pi f_0 t + (\phi_{\mathrm{path1}} - \phi_{\mathrm{path2}})\right) \\ &\quad + A_{\mathrm{Beam1}} A_{\mathrm{Beam2}} \Big/ \sqrt{2} \cos\left(\begin{array}{l} 2\pi f_0 t + (\phi_{\mathrm{path1}} - \phi_{\mathrm{path2}}) - \\ \left(\begin{array}{l} \phi_{\mathrm{offset}} + \phi_{\mathrm{modulate}} \\ \cos\left(2\pi f_{\mathrm{modulate}} + \phi_{m0}\right) \end{array}\right) \end{array}\right) \\ &\quad + A^2_{\mathrm{Beam2}} \Big/ 2 \cos\left(\phi_{\mathrm{offset}} + \phi_{\mathrm{modulate}} \cos\left(2\pi f_{\mathrm{modulate}} t + \phi_{m0}\right)\right). \end{aligned} \tag{2}$$

Equation (2) can be represented in terms of intensity, which is recorded as

$$\begin{aligned} P_{\mathrm{out}} &= I_{\mathrm{Beam1}} + I_{\mathrm{Beam2}} + \sqrt{2 I_{\mathrm{Beam1}} I_{\mathrm{Beam2}}} \cos(\varphi) \\ &\quad + \sqrt{2 I_{\mathrm{Beam1}} I_{\mathrm{Beam2}}} \cos\left(\begin{array}{l} \varphi - \\ \left(\begin{array}{l} \phi_{\mathrm{offset}} + \\ \phi_{\mathrm{modulate}} \cos(\varphi_m) \end{array}\right) \end{array}\right) \\ &\quad + I_{\mathrm{Beam2}} \cos\left(\phi_{\mathrm{offset}} + \phi_{\mathrm{modulate}} \cos(\varphi_m)\right) \\ &= I_{\mathrm{Beam1}} + I_{\mathrm{Beam2}} + \sqrt{2 I_{\mathrm{Beam1}} I_{\mathrm{Beam2}}} \cos(\varphi) \\ &\quad + \sqrt{2 I_{\mathrm{Beam1}} I_{\mathrm{Beam2}}} \cos\left(\varphi - \phi_{\mathrm{offset}}\right) \cdot \cos\left(\phi_{\mathrm{modulate}} \cos(\varphi_m)\right) \\ &\quad + \sqrt{2 I_{\mathrm{Beam1}} I_{\mathrm{Beam2}}} \sin\left(\varphi - \phi_{\mathrm{offset}}\right) \cdot \sin\left(\phi_{\mathrm{modulate}} \cos(\varphi_m)\right) \\ &\quad + I_{\mathrm{Beam2}} \cos\phi_{\mathrm{offset}} \cdot \cos\left(\phi_{\mathrm{modulate}} \cos(\varphi_m)\right) \\ &\quad - I_{\mathrm{Beam2}} \sin\phi_{\mathrm{offset}} \cdot \sin\left(\phi_{\mathrm{modulate}} \cos(\varphi_m)\right) \\ &= I_{\mathrm{Beam1}} + I_{\mathrm{Beam2}} + \sqrt{2 I_{\mathrm{Beam1}} I_{\mathrm{Beam2}}} \cos(\varphi) \\ &\quad + \sqrt{2 I_{\mathrm{Beam1}} I_{\mathrm{Beam2}}} \cos\left(\varphi - \phi_{\mathrm{offset}}\right) \cdot J_0(\phi_{\mathrm{modulate}}) \\ &\quad + \sqrt{2 I_{\mathrm{Beam1}} I_{\mathrm{Beam2}}} \left(2 \sum_{n=1}^{\infty} \left(\begin{array}{l} J_n(\phi_{\mathrm{modulate}}) \cos\left(\begin{array}{l} \varphi - \phi_{\mathrm{offset}} \\ + n\frac{\pi}{2} \end{array}\right) \\ \cdot \cos(n(\varphi_m + \pi)) \end{array}\right)\right) \\ &\quad + I_{\mathrm{Beam2}} \cos\phi_{\mathrm{offset}} \cdot J_0(\phi_{\mathrm{modulate}}) \\ &\quad + I_{\mathrm{Beam2}} \left(2 \sum_{n=1}^{\infty} \left(\begin{array}{l} J_n(\phi_{\mathrm{modulate}}) \sin\left((n+1)\frac{\pi}{2} + \phi_{\mathrm{offset}}\right) \\ \cdot \cos(n\varphi_m) \end{array}\right)\right), \end{aligned} \tag{3}$$

where I_{Beam1} and I_{Beam2} are the powers of two laser beams after the first BS; $\varphi = 2\pi f_0 t + (\phi_{\mathrm{path1}} - \phi_{\mathrm{path2}})$ and $\varphi_m = 2\pi f_{\mathrm{modulate}} t + \phi_{m0}$, $J_n(\phi_{\mathrm{modulate}})$ represent the Bessel function, respectively.

From Eq. (3), there are three types of signals in the last beat note: the main signal S_{Carrier}, the modulated signal, and its harmonics S_{Modulate} and the mixed part of the above signal S_{Mix}, which can be expressed by

$$\begin{aligned} S_{\mathrm{Carrier}} &= \sqrt{2 I_{\mathrm{Beam1}} I_{\mathrm{Beam2}} \cdot \left(\begin{array}{l} (1 + \cos\phi_{\mathrm{offset}} J_0(\phi_{\mathrm{modulate}}))^2 \\ + (\sin\phi_{\mathrm{offset}} \cdot J_0(\phi_{\mathrm{modulate}}))^2 \end{array}\right)} \cos(\varphi - \theta) \\ S_{\mathrm{Mix}} &= \sqrt{2 I_{\mathrm{Beam1}} I_{\mathrm{Beam2}}} \left(2 \sum_{n=1}^{\infty} \left(\begin{array}{l} J_n(\phi_{\mathrm{modulate}}) \cos\left(\begin{array}{l} \varphi - \phi_{\mathrm{offset}} \\ + n\frac{\pi}{2} \end{array}\right) \\ \cdot \cos(n(\varphi_m + \pi)) \end{array}\right)\right) \\ S_{\mathrm{Modulate}} &= I_{\mathrm{Beam2}} \left(2 \sum_{n=1}^{\infty} \left(\begin{array}{l} J_n(\phi_{\mathrm{modulate}}) \sin\left((n+1)\frac{\pi}{2} + \phi_{\mathrm{offset}}\right) \\ \cdot \cos(n\varphi_m) \end{array}\right)\right), \end{aligned} \tag{4}$$

where

$$\theta = \arccos \left(\frac{1 + \cos\phi_{\mathrm{offset}} J_0(\phi_{\mathrm{modulate}})}{\sqrt{(1 + \cos\phi_{\mathrm{offset}} J_0(\phi_{\mathrm{modulate}}))^2 + (\sin\phi_{\mathrm{offset}} \cdot J_0(\phi_{\mathrm{modulate}}))^2}}\right).$$

From Eq. (4), the main signal S_{Carrier} obtains the optical path information of the interferometer. Its amplitude is related with I_{Beam1}, I_{Beam2}, ϕ_{offset}, and ϕ_{modulate}. The modulation signal only has the information ϕ_{m0} of the modulated rf signal, which has no relationship with noises of the optical path. Therefore, the modulation signal S_{Modulate} gives an ideal choice of the OPT for the theme of the common-mode noise correction, which will be discussed in the following subsection. The mixed part S_{Mix} contains the optical path and the phase information ϕ_{m0} of the modulated signal implemented on the EOAM.

A. Optical Pilot Tone

The pilot tone is a kind of signal to correct the ADC sampling jitter noise in the phase measurement. Traditionally, an analog signal is added to the tested signal by a power combiner with the different frequency before the ADC sampling. The sampling noise is recorded, which is proportional to the frequency value of the signal. Moreover, the pilot tone not only can correct the jitter of the ADC sampling, but also the analog frontend noise of phasemeter. However, noises, which have the different transfer paths of the main signal and the analog pilot tone, cannot be rejected, such as the rf coaxial cable and the photodetector. Differently, compared with the analog pilot tone, the OPT mainly has two advantages: (1) The OPT has the same transfer path as the main signal, which leads to that almost all common-mode noises can be rejected. (2) The analog circuits of the power combiner/splitter, which add the analog signal to the main signal, can be removed. Fewer analog chips mean less imported noise. Therefore, The OPT is an ideal choice for the common-mode noise reject theme.

Back to Eq. (4), S_{Modulate} meets such characteristics of OPT. There are many tones of higher harmonics in the signal. The higher amplitude and lower frequency of the OPT are preferred. So, $n = 1$ is the best choice of the OPT in Eq. (4). For the largest amplitude, the following expression should be satisfied:

$$\sin\left(\pi + \phi_{\mathrm{offset}}\right) = \pm 1.$$

In the paper, we set $\phi_{\mathrm{offset}} = -\pi/2$. Therefore, the OPT is written as

$$S_{\mathrm{OPT}} = 2 I_{\mathrm{Beam2}}\, J_1(\phi_{\mathrm{modulate}}) \cdot \cos(\varphi_m).$$

The amplitude of the OPT is proportional to I_{Beam2} and $J_1(\phi_{\mathrm{modulate}})$. Moreover, Eq. (4) is simplified as

$$S_{\mathrm{Carrier}} = \sqrt{2 I_{\mathrm{Beam1}} I_{\mathrm{Beam2}} \cdot \left(1 + J_0^2(\phi_{\mathrm{modulate}})\right)}\cos\left(\varphi - \theta\right)$$

$$S_{\mathrm{Mix}} = \sqrt{2 I_{\mathrm{Beam1}} I_{\mathrm{Beam2}}}\left(2\sum_{n=1}^{\infty}\left(\begin{array}{l} J_n(\phi_{\mathrm{modulate}})\cos\left(\begin{array}{l}\varphi + \\ (n+1)\frac{\pi}{2}\end{array}\right) \\ \cdot\cos(n(\varphi_m + \pi))\end{array}\right)\right)$$

$$S_{\mathrm{Modulate}} = I_{\mathrm{Beam2}}\left(2\sum_{n=1}^{\infty}\left(\begin{array}{l} J_n(\phi_{\mathrm{modulate}})\sin\left(n\frac{\pi}{2}\right) \\ \cdot\cos(n\varphi_m)\end{array}\right)\right), \tag{5}$$

where $\theta = \arccos\left(\frac{1}{\sqrt{1+J_0^2(\phi_{\mathrm{modulate}})}}\right)$.

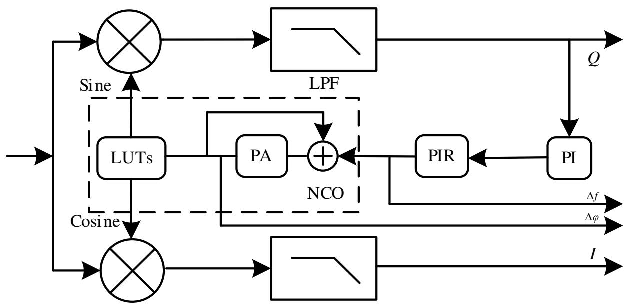

Fig. 2. Typical diagram of the DPLL architecture. Phase accumulator (PA), look-up table (LUT), numerically controlled oscillator (NCO), phase increment register (PIR), proportional integral (PI), and low-pass filter (LPF).

B. Phase Readout

From Eq. (4), we can find out that the signal of the CAM strategy is similar to the traditional heterodyne interferometry. Differently, there are multitones in the last signal. Therefore, the DPLL phase meter which is widely used in the space interferometer also can be used in the phase extraction of the CAM [16–18]. The typical diagram of the DPLL is shown in Fig. 2.

From Fig. 2, the DPLL consists of the NCO, the PIR, the multiplier, the LPF, and the PI controller. If the loop is locked, the DPLL is worked in the linear range. Through reading the PIR and PA values, the frequency and phase fluctuations is obtained, which is called the frequency readout and the PA readout. Through the readout of I, the amplitude of the tested signal is obtained in the end. By setting a proper initial frequency of the NCO, the DPLL can distinguish different tones in the signal.

C. Auxiliary Functions

The CAM utilizes the EOAM to modulate the amplitude of the laser, which changes the electric field on the phase modulating path. Therefore, the PRN and the communication code can also be encoded through the EOAM. The PRN code gives the CAM the ability to distinguish the multitargets in the laser transfer road [5,6,19]. The CAM not only can give an OPT for the noise rejection, but also can extend other auxiliary functions. Therefore, it is a good candidate for the design of optical layout in the gravitational wave detection mission, such as Taiji and LISA.

3. MODULATED PARAMETER OF CAM

The CAM is the best choice of the deep amplitude modulation. So, the modulated parameters, such as the modulation depth, the split ratio, and the modulated frequency selection, will be discussed in the following.

A. Modulation Depth

From Eq. (5), the amplitude of the S_{Carrier} and the S_{OPT} are $\sqrt{2 I_{\mathrm{Beam1}} I_{\mathrm{Beam2}} \cdot (1 + J_0^2(\phi_{\mathrm{modulate}}))}$ and $2 I_{\mathrm{Beam2}} J_1(\phi_{\mathrm{modulate}})$, respectively. For the phase measurement, different amplitude represents different signal-to-noise ratios, which leads to the different measurement noise floor. Therefore, the similar amplitude of two signals is required.

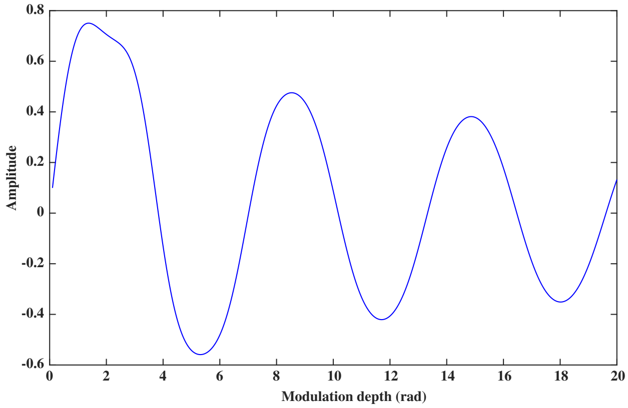

Fig. 3. Relationship between the amplitude and the modulation depth ϕ_{modulate}.

The ratio of two amplitude R's can be expressed by

$$R = \sqrt{2 I_{\text{Beam1}} I_{\text{Beam2}} \cdot \left(1 + J_0^2(\phi_{\text{modulate}})\right)} \Big/ \left(2 I_{\text{Beam2}} J_1(\phi_{\text{modulate}})\right)$$
$$= \sqrt{\frac{n}{2}} \cdot \sqrt{\left(1 + J_0^2(\phi_{\text{modulate}})\right)} \Big/ J_1(\phi_{\text{modulate}}), \tag{6}$$

where $n = I_{\text{Beam1}} / I_{\text{Beam2}}$ is the power splitting ratio of the beam splitter. From Eq. (6), R is related to n and the modulation depth ϕ_{modulate}. If we want to obtain a similar amplitude, R should be around 1. So, the following relationship is obtained:

$$n = 2 \frac{J_1^2(\phi_{\text{modulate}})}{1 + J_0^2(\phi_{\text{modulate}})}. \tag{7}$$

We also want to obtain the highest amplitude of the main signal and the OPT signal. The amplitude of the main signal can be expressed by

$$A = \sqrt{2 I_{\text{Beam1}} I_{\text{Beam2}} \cdot \left(1 + J_0^2(\phi_{\text{modulate}})\right)}$$
$$= \sqrt{2\left(1 + J_0^2(\phi_{\text{modulate}})\right)} \cdot I \frac{\sqrt{n}}{1 + n}$$
$$= 2I \frac{J_1(\phi_{\text{modulate}}) \cdot \left(1 + J_0^2(\phi_{\text{modulate}})\right)}{1 + J_0^2(\phi_{\text{modulate}}) + 2{J_1}^2(\phi_{\text{modulate}})}. \tag{8}$$

For convenience of calculations, normalized processing is adopted during the conversion from the laser power intensity to the output voltage of photodetector. Various sources of loss and gain in the system, such as the quantum efficiency and the amplifier gain, have been ignored. Importantly, the processing of normalization does not affect the optimal value analysis of modulation depth. Therefore, assuming the laser power $I = 1$, the relationship between the amplitude and the modulation depth is shown in Fig. 3.

From Eq. (8) and Fig. 3, the preferred modulated parameter of the CAM are the amplitude $= 0.7505$ and $\phi_{\text{modulate}} = 1.375$ rad, respectively. In this condition, the power ratio of the beam split $n = 0.432$. Considering the accurate values of ϕ_{modulate} and n are hard to achieve, a 1% error of amplitude ratio R is acceptable in the actual experiment. From Eq. (6), the permissive ranges of ϕ_{modulate} and n are 1.367–1.383 and 0.427–0.437, respectively.

B. Nonlinearity

From the former discussion, the best modulation depth is 1.375 rad, which is deep enough. So, the nonlinearity of the CAM should be discussed. Figure 4 gives the relationship between $J_n(\phi_{\text{modulate}})$ and n with different modulation depths ϕ_{modulate}.

In Fig. 4, the higher harmonics cannot be ignored with the modulation depth becoming large. If the modulated phase $= 1.375$ rad, at least, three harmonics cannot be ignored. In this condition, the amplitude spectrum of the heterodyne signal is given by Fig. 5.

From Fig. 5, the nonlinearity of the CAM signal becomes more and more obvious along with the modulation depth enlarge. There are, at least, nine frequency signals in the last beat note, including the main part, the OPT, and its higher harmonics, and the mixed part of the above signal. The phase meter should face multitones, and those tones are not mixed with each other. Moreover, the DPLL should have the ability to distinguish the tones. The capture frequency of the DPLL is written as F_{Loop}. If the difference of two frequencies is small than this value, the DPLL cannot distinguish with each other. Therefore, the proper selection of f_0 and f_{modulate} should be discussed.

C. Modulated Frequency

In the CAM, there are three types of frequency f_0, $n f_{\text{modulate}}$, and $f_0 \pm n f_{\text{modulate}}$ in the ending signal. To avoid the overlap of different frequencies, there are several limitations in the selection of frequencies,

$$|f_0 - n f_{\text{modulate}}| \geq F_{\text{Loop}}$$
$$|f_{\text{modulate}} - (f_0 + n f_{\text{modulate}})| \geq F_{\text{Loop}}$$
$$|f_{\text{modulate}} - (f_0 - n f_{\text{modulate}})| \geq F_{\text{Loop}}$$
$$f_{\text{modulate}} \gg F_{\text{Loop}}$$
$$f_0 \gg F_{\text{Loop}}, \tag{9}$$

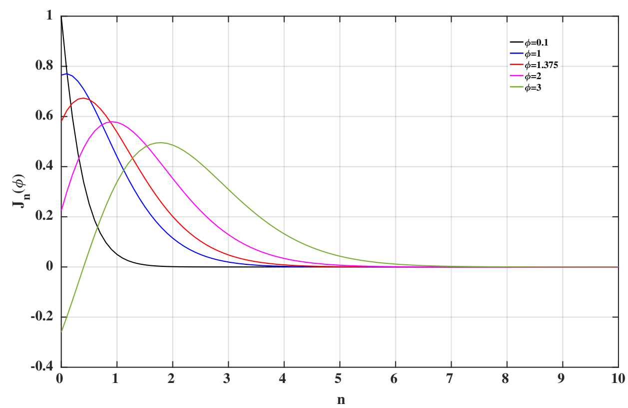

Fig. 4. Relationship of n and J_n with different modulation depths.

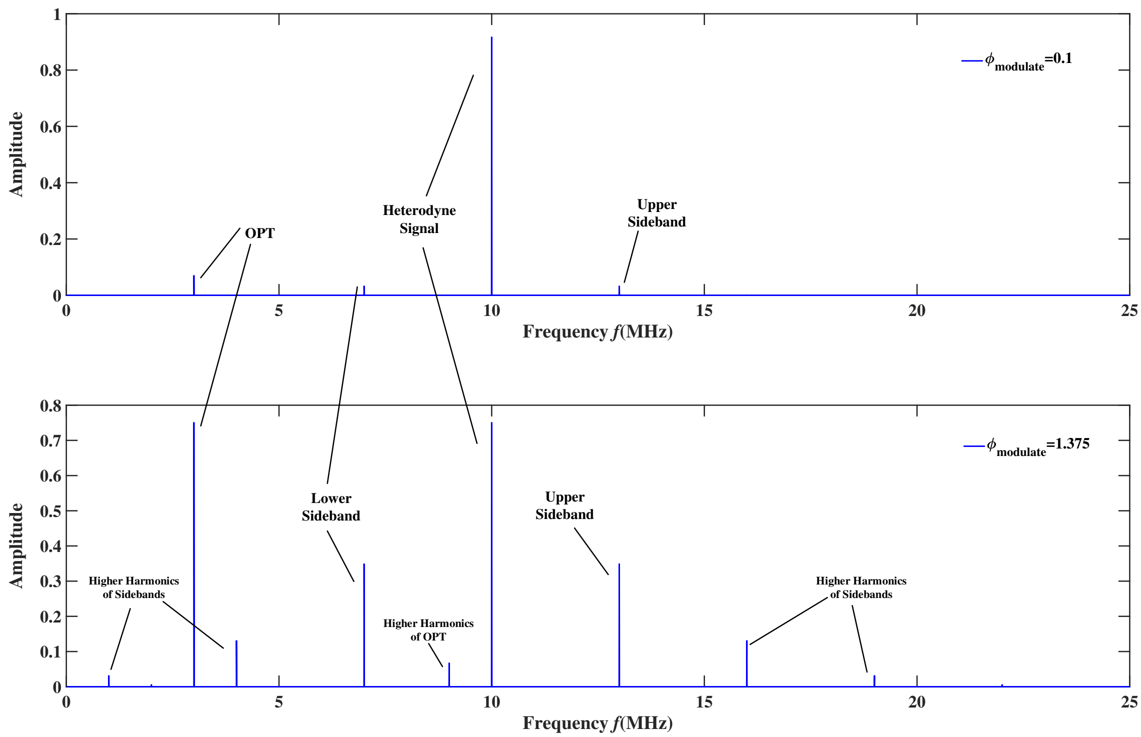

Fig. 5. Amplitude spectrum of the CAM with $n = 0.432$ and different ϕ_{modulate}'s where the heterodyne frequency is 10 MHz with 3-MHz amplitude modulation.

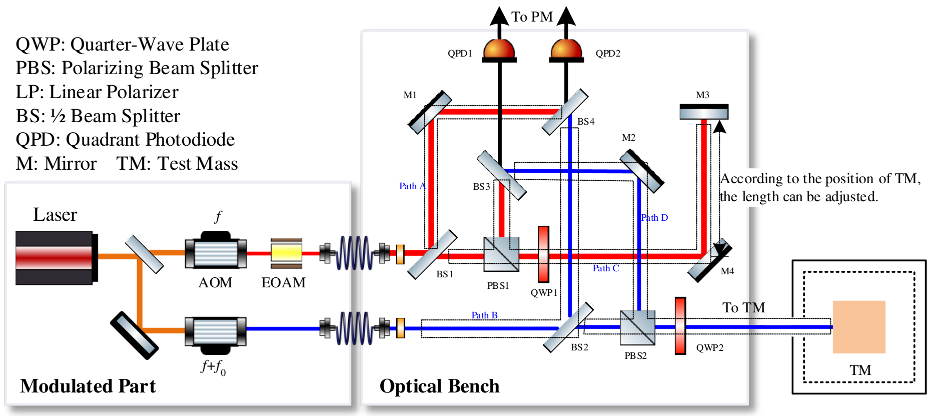

Fig. 6. Optical layout of the simulated case.

where $n = 1 - 3$, $F_{\text{Loop}} \geq 0$, $f_{\text{modulate}} \geq 0$. Equation (9) can be simplified as

$$|f_0 - n f_{\text{modulate}}| \geq F_{\text{Loop}}$$
$$f_{\text{modulate}} \gg F_{\text{Loop}}$$
$$f_0 \gg F_{\text{Loop}}. \tag{10}$$

F_{Loop} is always around the order of 10 kHz. f_0 is always about 2–20 MHz in the space mission [15]. f_{modulate} is always set as two to five times smaller than f_0.

4. SIMULATION AND DISCUSSION

As to investigate the performance of the CAM interferometry strategy, a simulated case has been implemented as shown in Fig. 6.

In Fig. 6, an implementable optical layout for the TM readout is displayed. The optical layout mainly has two parts: a modulated part and an optical bench. A laser beam is first split into two, and then frequency shifted by two AOMs with different values. One of the beams further passes through an EOAM. Then, two modulated beams are imported into the optical bench by the optical fiber. Through different lens, two interferometers are formed: one for the reference and the other for the TM measurement. f_0, f_{modulate}, ϕ_{modulate}, and n are set as 10, 3 MHz, and 1.375 rad, 0.432, respectively. According to the

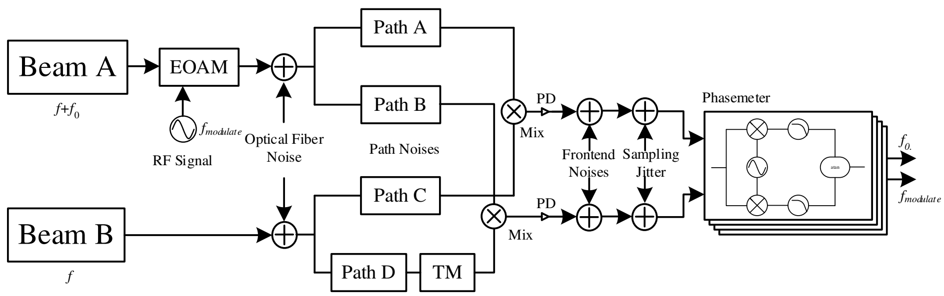

Fig. 7. Simulation program diagram of the simulated case.

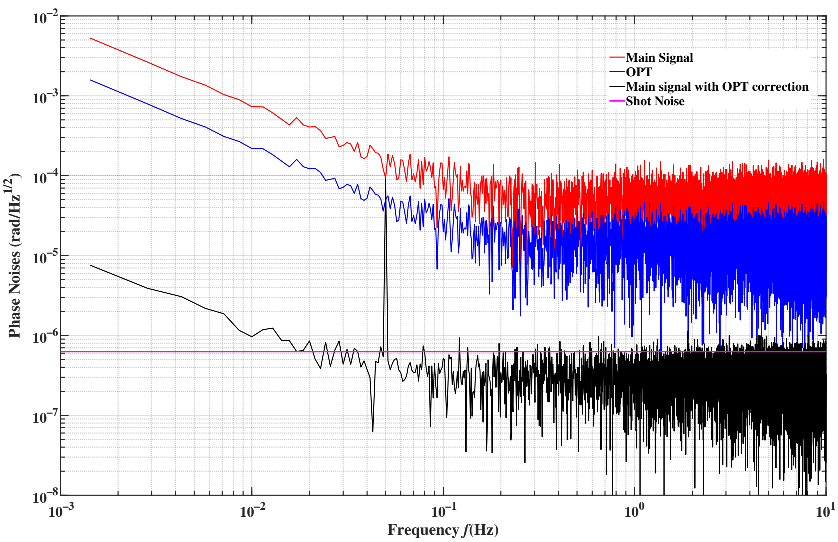

Fig. 8. Results of the simulation case.

optical layout, the simulated program diagram by MATLAB of the simulation case is shown in Fig. 7.

In Fig. 7, the simulation is based on the actual physical process where all possible noises are considered in the program. Beam A and beam B express the laser beams after AOMs with different frequency values. Then, beam A is amplitude modulated by the EOAM, driven by the rf signal. The crystal of the EOAM ($LiNbO_3$) and the following optical fiber are easily affected by the environment, such as the temperature and the vibration. Paths A–D are the corresponding optical path shown in Fig. 6. Path noises are also produced by the environment of the optical bench. The whole lens is installed in one plate, which has an ultralow expansion coefficient (Invar steel or Zerodur). Therefore, the common mode noise, such as the thermal or the vibration, can be well rejected. The information of the TM motion can be well obtained. In the simulation, a sinusoidal motion with 0.05 Hz has been given to the TM. The photodetector is a device to transfer the interferometric signal into the electric signal, which will introduce the shot noise ($2\pi \times 10^{-7}$ rad/Hz$^{1/2}$) and electronic noise. The analog front end is mainly composed of the antialiasing filter, the rf amplifier, the rf transformer, the transmission line, etc. The phase response of the signal in the analog circuits is easily influenced by the environmental temperature. The sampling jitter is produced by the ADC sampling jitter (1 to 2 ps/Hz$^{1/2}$) and can be rejected by the pilot tone.

Results of the simulation are shown in Fig. 8.

From Fig. 8, the main signal (red line) records all information, including optical path noises, shot noise, the noise of the PD, the analog frontend noise, and the sampling jitter. Before the OPT correction, the limited noises of the main signal are the sampling jitter and the thermal noise of the optical bench. Sampling jitter mainly dominates the noise in the frequency range of 0.1 and 10 Hz. Thermal noise restricts the performance in the frequency below 0.1 Hz. The TM motion is also submerged below the noise floor. The OPT (blue line) only records the noise of the PD, the analog frontend noise, and the ADC sampling jitter. Comparing the main signal with OPT, the noise level of lines linearly enlarges with the frequency value increasing. It is because that the part noise of the PD, the thermal drift noise of the analog frontend and the ADC sampling jitter are linearly enlarged with the frequency increasing. Using the OPT to correct the result of the main signal (black line), the limited noise in the frequency of 0.01 and 10 Hz is changed to shot noise ($2\pi \times 10^{-7}$ rad/Hz$^{1/2}$). But the limited noise in the frequency below 0.01 Hz is the remained thermal noise of optical bench, which is the differential mode part. Importantly, the information of TM motion has appeared. Therefore, the phenomenon of the simulation agrees with Eq. (5) and verifies the validity of the CAM strategy.

5. CONCLUSION AND OUTLOOK

In this paper, the CAM interferometry strategy has been proposed and discussed. Compared with other interferometry methods, the CAM has fewer sidebands, and the phase extraction method can be inherited from the DPLL structure. Importantly, the CAM interferometry offers the OPT for the further noise correction theme. Compared with the rf analog pilot tone, the OPT not only can correct the ADC sampling jitter, but also noises of the PD and the analog front-end noise (including the rf coaxial cable). From the discussion, $\phi_{\text{modulate}} = 1.375$, the power ratio of the BS $n = 0.432$ is the best choice of the CAM-modulated parameter. Moreover, a simulated case has been implemented for the verification of the CAM. In the next, the demonstrated experiment of the CAM heterodyne interferometry will be prepared and implemented for further research.

Funding. National Key Research and Development Program of China (2020YFC2200104, 2021YFC2202902).

Disclosures. The authors declare no conflicts of interest.

Data availability. Data underlying the results presented in this paper are not publicly available at this time but may be obtained from the authors upon reasonable request.

REFERENCES

1. S. Vitale, “Space-borne gravitational wave observatories,” Gen. Relativ. Gravit. **46**, 1–19 (2014).
2. W.-R. Hu and Y.-L. Wu, “The Taiji program in space for gravitational wave physics and the nature of gravity,” Natl. Sci. Rev. **4**, 685–686 (2017).
3. K.-S. Isleif, G. Heinzel, M. Mehmet, and O. Gerberding, “Compact multifringe interferometry with subpicometer precision,” Phys. Rev. Appl. **12**, 034025 (2019).
4. S. P. Francis, T. T.-Y. Lam, D. E. McClelland, and D. A. Shaddock, “Multi-link laser interferometry architecture for interspacecraft displacement metrology,” J. Geod. **92**, 241–251 (2017).
5. D. A. Shaddock, “Digitally enhanced heterodyne interferometry,” Opt. Lett. **32**, 3355–3357 (2007).
6. A. J. Sutton, O. Gerberding, G. Heinzel, and D. A. Shaddock, “Digitally enhanced homodyne interferometry,” Opt. Express **20**, 22195–22207 (2012).
7. K.-S. Isleif, O. Gerberding, S. Köhlenbeck, A. Sutton, B. Sheard, S. Goßler, D. Shaddock, G. Heinzel, and K. Danzmann, “Highspeed multiplexed heterodyne interferometry,” Opt. Express **22**, 24689–24696 (2014).
8. G. Heinzel, F. G. Cervantes, A. F. G. Marín, J. Kullmann, W. Feng, and K. Danzmann, “Deep phase modulation interferometry,” Opt. Express **18**, 19076–19086 (2010).
9. O. Gerberding, “Deep frequency modulation interferometry,” Opt. Express **23**, 14753–14762 (2015).
10. K.-S. Isleif, O. Gerberding, T. S. Schwarze, M. Mehmet, G. Heinzel, and F. G. Cervantes, “Experimental demonstration of deep frequency modulation interferometry,” Opt. Express **24**, 1676–1684 (2016).
11. K.-S. Isleif, O. Gerberding, M. Mehmet, T. S. Schwarze, G. Heinzel, and K. Danzmann, “Comparing interferometry techniques for multi-degree of freedom test mass readout,” J. Phys.: Conf. Ser. **716**, 012008 (2016).
12. T. S. Schwarze, O. Gerberding, F. G. Cervantes, G. Heinzel, and K. Danzmann, “Advanced phasemeter for deep phase modulation interferometry,” Opt. Express **22**, 18214 (2014).
13. O. Gerberding, B. Sheard, I. Bykov, J. Kullmann, J. J. E. Delgado, K. Danzmann, and G. Heinzel, “Phasemeter core for intersatellite laser heterodyne interferometry: modelling, simulations and experiments,” Class. Quantum Grav. **30**, 235029 (2013).
14. D. Shaddock, B. Ware, P. Halverson, R. E. Spero, and B. Klipstein, “Overview of the LISA phasemeter,” AIP Conf. Proc. **873**, 654–660 (2006).
15. K. Danzmann, “LISA mission overview,” Adv. Space Res. **25**, 1129–1136 (2000).
16. G. Heinzel, M. D. Álvarez, A. Pizzella, N. Brause, and J. J. E. Delgado, “Tracking length and differential-wavefront-sensing signals from quadrant photodiodes in heterodyne interferometers with digital phase-locked-loop readout,” Phys. Rev. Appl. **14**, 054013 (2020).
17. H.-S. Liu, T. Yu, and Z.-R. Luo, “A low-noise analog frontend design for the Taiji phasemeter prototype,” Rev. Sci. Instrum. **92**, 054501 (2021).
18. L. E. Roberts, “Internally sensed optical phased arrays,” Ph.D. thesis (Australian National University, 2016).
19. P. G. Sibley, R. L. Ward, L. E. Roberts, S. P. Francis, and D. A. Shaddock, “Crosstalk reduction for multi-channel optical phase metrology,” Opt. Express **28**, 10400–10424 (2020).